Chemical Science

Accepted Manuscript

This article can be cited before page numbers have been issued, to do this please use: S. Mandal, C. Priyanka, A. Karmakar, R. K. Aparna, L. Singh, P. K. Mondal, S. Kundu and K. Bhattacharyya, *Chem. Sci.*, 2025, DOI: 10.1039/D4SC08408J.

ROYAL SOCIETY OF CHEMISTRY

rsc.li/chemical-science

View Article Online
DOI: 10.1039/D4SC08408J

ARTICLE

Linker Driven Site-specific Catalysis in Atomically Precise Silver Cluster-Assemblies

Received 00th January 20xx,
Accepted 00th January 20xx

DOI: 10.1039/x0xx00000x

Priyanka Chandrashekar,[a] Arun Karmakar,[b] Ravari Kandy Aparna,[a] Laddi Singh,[c] Pradip Kumar Mondal,[d] Subrata Kundu,[b] Kalishankar Bhattacharyya,[c*] Sukhendu Mandal [a *]*

Metal nanoclusters (NCs) exhibit potential as catalysts for electrochemical studies, providing atomic-level insights into mechanisms. However, it remains elusive to construct an integrated catalyst with a molecular-level understanding of its mechanism, especially in silver cluster assemblies. In this study, we have shown that atomically precise Ag_{12} cluster assemblies Ag_{12}-py, Ag_{12}-pyz, Ag_{12}-bpy, Ag_{12}-bpa, Ag_{12}-azopy, (where Ag_{12} = secondary building unit, Py = pyridine, pyz = pyrazine, bpy = 4,4′-Bipyridine, bpa = 1,2-Bis(4-pyridyl)ethane, azopy = 4,4′-Azopyridine), serve as paradigms for demonstrating the hydrogen evolution reaction (HER), where the catalytic activity is fine-tuned by two functional units: the cluster core and the linkers. Atomic resolution of such catalysts permits tracing the reaction process *via* experiments coupled with theory and structural analysis. Site-specific catalysis for Ag_{12}pyz induced by metal cluster assembly & linker synergy can be accurately elucidated to dominate in the series. Taking advantage of pyrazine linker for its less basicity and isotropic nature of inter-cluster interactions in Ag_{12}-pyz, it shows enhanced catalytic activity and selective hydrogen adsorption at the sulfur site, different from others in the series with nearly five times higher efficiency. This work on a series of silver cluster assemblies provides a substantial structural model to understand the catalyst's active site and activity, further driving advancements in functional cluster-based assemblies.

Introduction

Atomically precise noble metal nanoclusters (NCs) which bridge molecular organometallic complexes and plasmonic metal nanoparticles (NPs),[1,2] comprising of few atoms, allow excellent control over the total structure, that exhibit unique electronic and optical properties, including molecular-like transitions, tunable photoluminescence, and high catalytic activity.[3,4,5] The manipulation of these properties is primarily achieved through control over the cluster core and protective ligands. The distinctive geometry and electronic structure make them particularly attractive in catalysis, due to their high surface-to-volume ratio, atomic precision structure, rich surface chemistry, and low coordination number. [5,6,7,8] These clusters can indeed be used as ideal model catalysts for correlating catalytic properties with their atom packing structures.[9,10,11,12,8] However, the major challenge is the insufficient stability leading to aggregation. Therefore it requires strategies to stabilize NC structures while preserving cluster integrity.[13,14,15,16]

To address these challenges, recent progress in utilizing NCs as nanoscale building blocks for superstructures[17,18,19] through assembly processes by employing bridging ligands is achieved, known as cluster-assembled materials (CAMs).[20,21,22] These CAMs not only enhance the stabilization of NCs but also merge functionalities of NCs and linkers.[23] They exhibit superior properties, and multiple tunable components, compared to their cluster building blocks.[24,25,26] This approach provides a potential solution for stabilizing NCs while simultaneously enhancing catalytic performance by facilitating improved electron transport and chemical interactions between clusters.

Electrocatalytic hydrogen evolution reaction (HER) is a fascinating and sustainable strategy to produce molecular hydrogen, which is considered an excellent fuel for the future. Hydrogen has high energy density and produces water as the sole byproduct upon combustion, making it an ideal candidate to replace fossil fuels, which cause many detrimental environmental issues.[27,28,29] Despite the inherent inertness or low HER activity of coinage metals such as gold, silver, and copper, the nanoscale regime introduces distinctive material properties, deviating from their bulk counterparts and offering potential avenues for enhanced catalytic activity. [30,31,32,33,34]

Ligand-protected metal NCs, such as Ag, Au, and Pt, have been minimally explored as catalysts,[13,35,36,37,38,39] and their assembled materials remain largely unstudied.[40,41,42,43] A more in-depth investigation is needed to understand the relationship between the structure of the electrocatalyst and catalytic

[a.] *School of Chemistry, Indian Institute of Science Education and Research Thiruvananthapuram, Kerala 69551, India. E-mail: sukhendu@iisertvm.ac.in*
[b.] *Electrochemical Process Engineering (EPE) Division, CSIR-Central Electrochemical Research Institute (CECRI), Karaikudi, Tamil Nadu, India-630006. Email: kundu.subrata@gmail.com*
[c.] *Department of Chemistry, IIT Guwahati, Assam, India-781039. E-mail: ksb@iitg.ac.in*
[d.] *Elettra-Sincrotrone Trieste, S.S. 14 Km 163.5 in Area Science Park, Basovizza, Trieste, Italy- 34149.*
†Electronic Supplementary Information (ESI) available. See DOI: 10.1039/x0xx00000x

DOI: 10.1039/D4SC08408J

performance at the atomic level.[44,45,46,47,48,49,50] Clusters with identical surface ligands and core atoms, but differing linkers, offer a unique opportunity to isolate and study the factors influencing overall performance. In this context, we focus on the synthesis and catalytic application of five silver cluster assemblies such as Ag_{12}-py $\{[Ag_{12}(C_6H_{11}S)_6(CF_3COO)_6(C_5H_5N)_6].4H_2O\}_n$,[25] Ag_{12}-pyz $[Ag_{12}(C_6H_{11}S)_6(CF_3COO)_6(C_4H_4N_2)_3]_n$, Ag_{12}-bpy $[Ag_{12}(C_6H_{11}S)_6(CF_3COO)_6(C_{10}H_8N_2)_3]_n$, Ag_{12}-bpa $[Ag_{12}(C_6H_{11}S)_6(CF_3COO)_6(C_{12}H_{12}N_2)_3(DMF)_2]_n$, and Ag_{12}-azopy $[Ag_{12}(C_6H_{11}S)_6(CF_3COO)_6(C_{10}H_8N_4)_3(DMF)_2]_n$. By working with precise Ag_{12} structured systems, we obviated the problem of accurately analyzing the origin for the difference in the catalytic activities, which plagues the study in structure-catalysis analysis. These assemblies exhibit varying activity levels, where the gradual lengthening of ligand systems from pyridine to azopyridine alters cluster arrangement. Ag_{12}-pyz CAM displayed very good catalytic performance for HER even under lower over-potentials. The low basicity of the pyrazine linker increases the electropositivity of the silver atom, shifting the catalytic active site from silver to sulfur. We propose that the linker basicity and assembly-induced cluster arrangements in these five assemblies define the active center and activity. This structure-property correlation, combined with experimental and theoretical insights, offers a promising model for cluster chemistry and electrocatalysis research.

Results and discussion

The Ag_{12}-py, Ag_{12}-pyz, Ag_{12}-bpy, Ag_{12}-bpa, and Ag_{12}-azopy, were prepared by a "one pot method". The $(Ag\text{-}SCy)_n$ (SCy-cyclohexanethiol) and $AgCF_3COO$ precursors were dissolved in solvent, followed by a dropwise addition of different linkers to yield five distinct assembly patterns: 2 three-dimensional extended Ag_{12}-pyz & Ag_{12}-bpa CAM and 2 two-dimensional extended Ag_{12}-bpy and Ag_{12}-azopy CAM; created by covalently linking the clusters with bidentate linkers (pyz = pyrazine, bpy = 4,4'-Bipyridine, bpa = 1,2-Bis(4-pyridyl)ethane, azopy = 4,4'-Azopyridine). The inter-cluster distance and dimensionality depends on the linker length and flexibility. Long rigid linkers, such as bpy and azopy, tend to facilitate two-dimensional assemblies (Figures 1 & 2). In contrast, more flexible linkers like bpa and the shorter rigid pyz linker promote the formation of three-dimensional structures. Non-covalent interactions extended the clusters with monodentate pyridine in Ag_{12}-py (py= pyridine) (Figure 1).

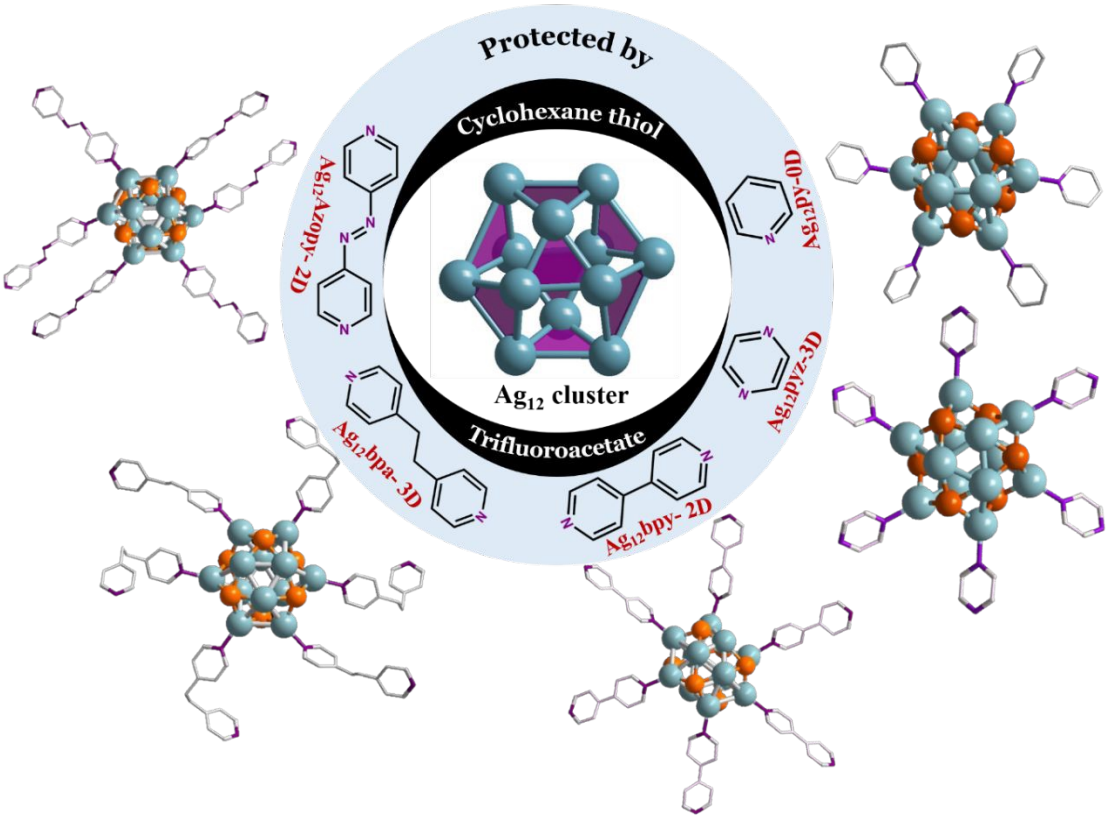

Fig. 1. (a) Schematic representation (cluster core with the linker) of five silver nanocluster assemblies. The core constituting Ag_{12} (center) is protected by cyclohexane thiol and trifluoroacetate ligand. The assemblies (right to left) Ag_{12}-py (0D NC), Ag_{12}-pyz (3D CAM), Ag_{12}-bpy (2D), Ag_{12}-bpa (3D), Ag_{12}-azopy (2D). The color code: Ag-blue, S-orange, N-violet, C-grey. All O, F, and H atoms are omitted for clarity.

View Article Online
DOI: 10.1039/D4SC08408J

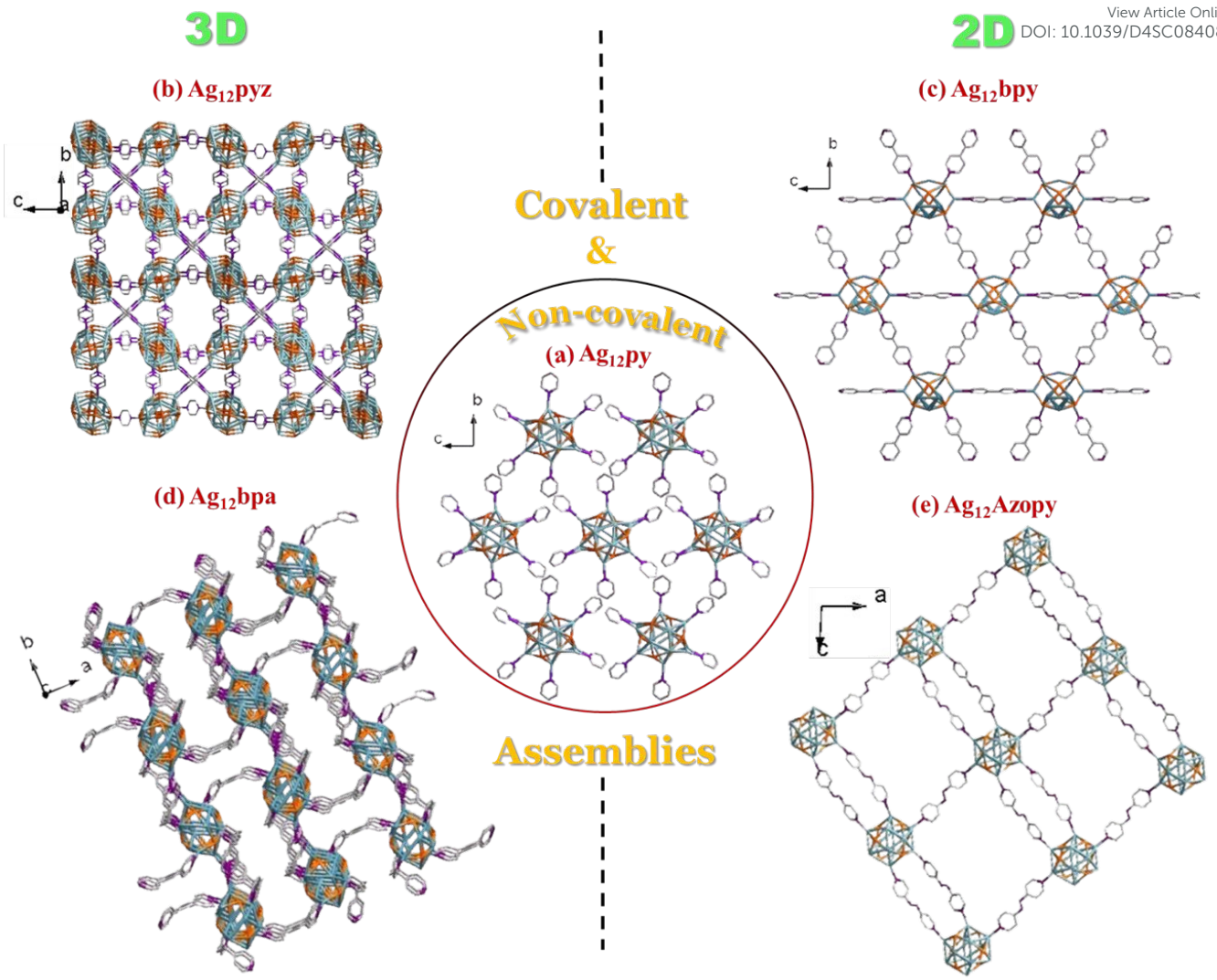

Fig. 2. Schematic representation of the four covalent (covalent bonding between the Ag of the cluster and N of the different N-based linkers) and a non-covalent assemblies. (a) Ag_{12}-py NC extends *via* non-covalent interactions by pyridine ligand, viewed along a direction. (b) Ag_{12}-pyz, the Ag_{12} clusters extend in three dimensions, the figure is viewed along *a* direction and slightly tilted to see the three-dimensional representation. (c) Ag_{12}-bpy, bpy linker extends the cluster in two two-dimensional hexagonal-like representations viewed along a direction. (d) Ag_{12}-bpa, the flexibility of the bpa linker extends the cluster three-dimensionally which is viewed along *c* direction and slightly tilted to see the assembly extend in *c* direction. (e) Ag_{12}-azopy, the azopy linker extends the cluster two-dimensionally which is viewed along *b* direction. The color code: Ag-blue, S-orange, N-violet, C-grey. All O, F, and H atoms are omitted for clarity.

Single Crystal X-Ray Diffraction (SCXRD) data of Ag_{12}-pyz crystals (Table S1, Figure S1a): crystallizes in *Pn*-3 (201), space group with the unit formula $[Ag_{12}(C_6H_{11}S)_6(CF_3COO)_6(C_4H_4N_2)_3]_n$. The cluster core constitutes of 12 Ag atoms held together by twelve argentophilic interactions with ~Ag…Ag distance of 2.93 Å (Table S5) which is protected by primary six cyclohexane thiol group in μ^4 fashion with Ag-S distance ~ 2.51 Å and six auxiliary CF_3COO^- ligands *via* oxygen in μ^2-η^2 mode with Ag-O distance ~ 2.40-2.51 Å. This $Ag_{12}(C_6H_{11}S)_6(CF_3COO)_6$ node connects with 6 pyrazine linkers *via* Ag-N bonds (~2.30 Å) (Figure S2) to further connects 6 other clusters (Figure S3). A simple topology of this can be viewed in Figure S4 which repeats itself in three dimensions (Figure 2b). The shortest Ag…Ag distance between two clusters in all three crystallographic directions is 7.40 Å (Figure S5).

The Ag_{12}-bpy, crystalized in *Pnnm* (No. 58) space group (Table S2 and Figure S1b), with the cluster unit formula $[Ag_{12}(C_6H_{11}S)_6(CF_3COO)_6(C_{10}H_8N_2)_3]_n$. The 12 Ag atoms which constitute the core are held by 20 argentophilic interactions (~ Ag…Ag distance of 3.15 Å) (Table S5). The silver core is protected by 6 cyclohexane thiol (Ag-S distance~ 2.47 Å) and six CF_3COO^- ligands (Ag-O distance ~ 2.20- 2.67 Å) in a similar fashion and further connected by six 4, 4' –dipyridyl linker (Figure S6) (Ag-N bonds ~2.24- 2.30 Å) to form two-

View Article Online
DOI: 10.1039/D4SC08408J

dimensionally extended solid (Figures 2c & S7), with the shortest Ag …Ag distances between two clusters in *bc* plane are 11.57 and 11.38 Å (Figure S8).

The Ag_{12}-bpa $[Ag_{12}(C_6H_{11}S)_6(CF_3COO)_6(C_{12}H_{12}N_2)_3(DMF)_2]_n$, crystallized in *C2/c* (No. 15) space group (Table S3 and Figure S1c). The core which is constituted of 12 silver atoms are held together by 18 argentophilic interactions (~Ag…Ag distance of 3.10 Å) (Table S5). The 6 cyclohexane thiol and 6 trifluoroacetate protects the cluster in a similar fashion (Ag-S distance~ 2.49 Å, Ag-O distance ~ 2.43- 2.75 Å). The bpa linker *via* Ag-N bonds (~2.27- 2.29 Å) connects each cluster to six others (Figure S9 & S10) to form a three-dimensionally extended solid (Figures 2d), with the shortest Ag…Ag distances between the neighboring cluster in the *bc* plane are 9.89 and 12.02 Å (Figure S11).

The Ag_{12}-azopy $[Ag_{12}(C_6H_{11}S)_6(CF_3COO)_6(C_{10}H_8N_4)_3(DMF)_2]_n$, crystallized in *C2/c* (No. 15) space group (Table S4 and Figure S1d). The 12 Ag atoms constituting the cluster core are held by 20 argentophilic interactions (~Ag…Ag distance of 3.15 Å) (Table S5). The cyclohexane thiol and trifluoroacetate ligands protect the cluster, this is further covalently linked by 6 azopy linkers (Figure S12) to form a two-dimensionally extended solid (Figures 2e & S13). The shortest Ag…Ag distances with the neighbouring clusters in the *ac* plane are 13.36 and 13.46 Å (Figure S14).

The Ag_{12}-NC, $\{[Ag_{12}(C_6H_{11}S)_6(CF_3COO)_6(C_5H_5N)_6].\ 4H_2O\}$ the non-covalently extended solid which is protected by pyridine (Figures 2a & S15-S16), was earlier synthesized by us.[25] This aids in correlating with the four new, two & three-dimensionally extended solids (Figures 1 & 2). Overall, five assemblies having a similar metal core and protecting ligands, differing in their assembly pattern have been studied, with the shortest intercluster distance in Ag_{12}-pyz and the longest in Ag_{12}-azopy, based on the linker connecting them. More compact assemblies or higher dimensional structures tend to show shorter Ag…Ag inter and intra-cluster distances. The shortest linker pyz connecting the clusters three-dimensionally (Ag_{12}-pyz), not only has reduced inter-cluster Ag…Ag distances but also reduced intra-cluster Ag…Ag distance and the series can be found in Table S6. Covalent assemblies offer a tunable approach to achieving desired structural compactness, which is less controllable in non-covalent assembly.

The Powder X-ray Diffraction (PXRD) pattern verified the crystallinity and phase purity of all the bulk samples, the resulting unaltered pattern indicates its structural stability (Figures S17-S21). The Scanning Electron Microscopic (SEM) images of Ag_{12}-pyz show octahedral morphology (Figure S22), Ag_{12}-bpy & Ag_{12}-azopy show hexagonal morphology (Figures S23 & S25), Ag_{12}-bpa has a block-like morphology (Figure S24), all of which are similar to their optical microscope images (Figure S1). The chemical composition of these samples was validated by SEM Energy-Dispersive X-ray Spectroscopy (EDS) analysis confirming the presence of all the elements (Figures S22-S25). X-ray Photoelectron Spectroscopy (XPS) analysis further elucidated the chemical identity and oxidation state of the respective elements in all the samples (Figures S26-S29). The survey spectra confirmed the presence of all the desired elements, namely Ag, S, N, O, and F. The binding energies of Ag $3d_{5/2}$ and Ag $3d_{3/2}$ were 368.85 eV and 374.85 eV for Ag_{12}-pyz, 368.57 eV and 374.57 eV for Ag_{12}-bpy, 368.37 eV and 374.37 eV for Ag_{12}-bpa, 368.59 eV and 374.59 eV for Ag_{12}-azopy, respectively, which affirms the presence of silver in the +1 oxidation state. Furthermore, the binding energy of S approximately at 163 eV, indicates the presence of bridging sulfur. The four CAM structures (Ag_{12}-pyz, Ag_{12}-bpy, Ag_{12}-bpa & Ag_{12}-azopy) exhibit enhanced thermal stability up to ~130 ℃ as determined by thermogravimetric analysis (TGA) (Figure S30a), However, they display varying degrees of thermal structural integrity at elevated temperatures, as indicated by PXRD analysis (Figure S30b). Ag_{12}-pyz assembly exhibits enhanced structural stability at higher temperatures.

View Article Online
DOI: 10.1039/D4SC08408J

ARTICLE

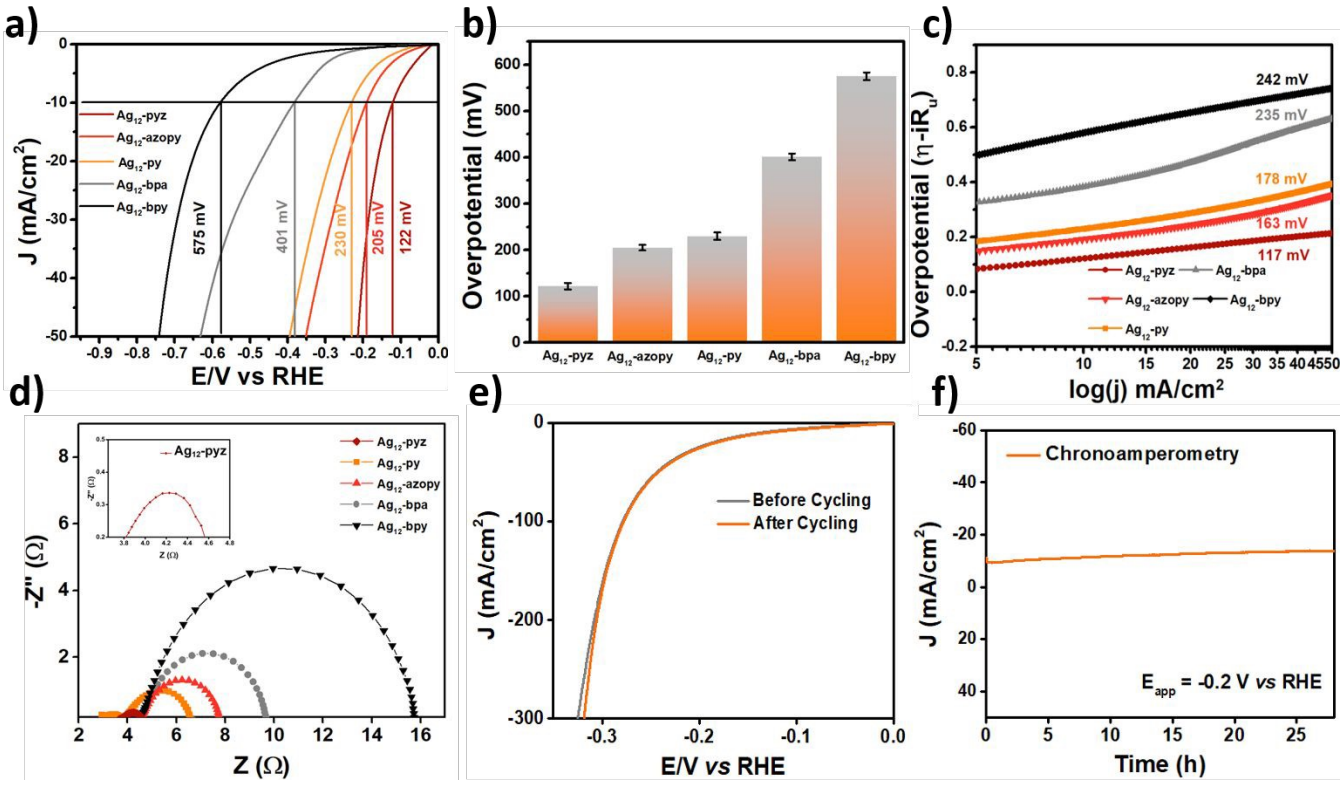

Fig. 3. HER performance of the catalysts. a) LSV curves in the order: Ag_{12}-pyz, Ag_{12}-azopy, Ag_{12}-py, Ag_{12}-bpa, and Ag_{12}-bpy, b) bar diagram representing the current density at different overpotentials of Ag_{12}-pyz, Ag_{12}-azopy, Ag_{12}-py, Ag_{12}-bpa, and Ag_{12}-bpy, c) Tafel slopes of all the five assemblies, (d) Nyquist plots of all the structures (Inset: Ag_{12}-pyz), (e) polarization curves of Ag_{12}-pyz before and after 2000 cycles, and (f) chronoamperometry measurements for the stability.

The electrochemical studies were carried out in 0.5 M H_2SO_4 with pH = 0.3 as the electrolyte, all five assemblies were loaded on carbon cloth for fabricating the working electrode. Linear sweep voltammetric (LSV) analysis of the samples carried out at a scan rate of 5 mV sec^{-1} revealed the overpotentials of the materials at a current density of 10 mA/cm^2 (Figure 3a). It was observed that the Ag_{12}-pyz CAM delivers a much lower overpotential of 122 mV compared to Ag_{12}-azopy, Ag_{12}-py, Ag_{12}-bpa, and Ag_{12}-bpy which shows an overpotential of 205, 230, 401, and 575 mV, respectively to drive the same current density of 10 mA/cm^2. The studies regarding the current density-dependent activity of the materials were carried out by calculating the overpotential delivered by the material at different current densities. The obtained values are shown in the bar diagram (Figure 3b).

The charge transfer kinetics at the electrode-electrolyte interface were analyzed using Tafel slopes of the materials obtained from the iR-corrected LSV plots, which were found to be 117, 163, 178, 235, and 242 $mVdec^{-1}$ in the order of Ag_{12}-pyz, Ag_{12}-azopy, Ag_{12}-py, Ag_{12}-bpa, and Ag_{12}-bpy, respectively (Figure 3c). The values of the Tafel slopes suggest that Ag_{12}-pyz shows faster charge-transfer kinetics among all the samples and follows the Volmer-Heyrovsky mechanism with the Heyrovsky step as the rate-determining step.[51] Electrochemical impedance spectroscopic analysis revealed the charge transfer resistance (R_{ct}) at the electrode-electrolyte interface. The Ag_{12}-pyz showed an R_{ct} as low as 0.68 Ω, whereas, for the Ag_{12}-azopy, Ag_{12}-py, Ag_{12}-bpa, and Ag_{12}-bpy the R_{ct} values were found to be 3.1, 3.52, 5.1, 11.1 Ω, respectively (Figure 3d).

From the LSV, Tafel slope as well as R_{ct} analysis, it was observed that, among the five catalysts, Ag_{12}-pyz exhibits the better HER activity. We also conducted some experiments to analyze the

View Article Online DOI: 10.1039/D5SC08408J

stability of the Ag_{12}-pyz catalyst. The dynamic stability of the Ag_{12}-pyz was studied using accelerated degradation (AD) studies for 1000 cycles at 200 mVs^{-1} scan rate. The material was maintaining its stability after the AD process (Figure 3e). Chronoamperometric analysis carried out at a constant potential of -0.2 V, also proved the high static stability of the material for 28 hours (Figure 3f). The amount of silver in the electrolyte of chronoamperometric experiments was found to be 0.626 ppm using ICP-MS analysis which further corroborates the stability of the catalyst. The stability of Ag_{12}-pyz in water is shown in Figure S31. The post-catalytic PXRD of Ag_{12}-pyz coated on a carbon tape confirms the cluster is intact after the catalysis cycle (Figure S32). The SEM-EDS analysis and XPS survey spectrum also confirm the presence of all the necessary elements: Ag, S, O, N, and F after the catalysis cycle (Figures S33 & S34). The binding energy values of silver at 368.9 and 374.9 eV are similar to the pre-catalytic Ag_{12}-pyz CAM, which further confirms the silver oxidation state of +1 and also the catalyst stability.

To gain further insight into the observed catalytic activity, computationally we measured the hydrogen adsorption free energy (ΔG_H) as a descriptor for understanding HER reactivity.[52] Initially, we performed the adsorption of a hydrogen atom at various accessible sites among the Ag and S core atoms within the optimized clusters. The ΔG_H energies at different conformers of the clusters are depicted in Figures 4a & b. Based on the optimized structures after hydrogen adsorption, it is shown that except for the Ag_{12}-pyz, hydrogen adsorption at the Ag site is energetically favourable compared to the S site. In the Ag_{12}-azopy, Ag_{12}-py, Ag_{12}-bpa, and Ag_{12}-bpy clusters, hydrogen adsorption is more favourable by over 5.09, 6.8, 7.55, and 0.57 kcal/mol, respectively, at the bridge Ag-Ag sites compared to the S sites (Table 1). It is important to note that, according to the Sabatier principle, both highly exothermic and highly endothermic hydrogen adsorption are detrimental to HER. In contrast, the Ag_{12}-pyz shows hydrogen adsorption at the apical S sites and is energetically favourable by 5.8 kcal/mol compared to adsorption at the bridge Ag-Ag site. The calculated ΔG_H values from the optimized structures (Figure S35) are shown in Figures 4a and b, indicate that the Ag_{12}-pyz could exhibit more effective HER activity compared to others, aligning well with the experimentally measured overpotential values.

These energetic differences are further corroborated by the observation that the apical S sites in the Ag_{12}-pyz cluster exhibit a higher negative charge, making them more prone to hydrogen adsorption compared to those in other analogues. After hydrogen adsorption to the S sites in Ag_{12}-pyz, computed Bader charges indicate that it carries a negative charge (~-0.155e), suggesting a greater electronic interaction of H with the sulphur active site than others. For the Ag_{12}-py, Ag_{12}-bpy, Ag_{12}-bpa, and Ag_{12}-azopy, charges of hydrogen adsorbed on the S sites are -0.145e, -0.133e, -0.150 e, and -0.133e, respectively. Changes in the linker within assemblies can influence basicity, which in turn affects catalytic activity. Specifically, linkers with higher basicity, such as py, bpa, and azopy, increase the electron density at Ag sites. This enhancement in electron density favors hydrogen binding at the Ag sites while reducing adsorption at the S sites. Overall, the trends in the binding energy at the S sites and the lower basicity of pyz result in superior performance in HER reactions compared to other linkers. It is important to note that the large negative charge density on the adsorbed S-H sites indicates the favourable charge transfer occurring from the catalyst surface to the adsorbed hydrogen. Hydrogen desorption would likely occur by the further adsorption of a proton from the electrolyte solution, followed by electron transfer, in a process known as the 'Heyrovsky' pathway. Adsorption of an additional hydrogen atom (Figure S36) in these clusters is energetically more favourable than the adsorption of a single hydrogen atom, further indicating that the HER follow the Volmer-Heyrovsky pathway as suggested by the Tafel slope analysis. Interestingly, the binding energy of the second hydrogen over the Ag_{12}-pyz cluster is less stable compared to the other studied clusters, resulting in superior HER activity as observed experimentally.

View Article Online
DOI: 10.1039/D4SC08408J

ARTICLE

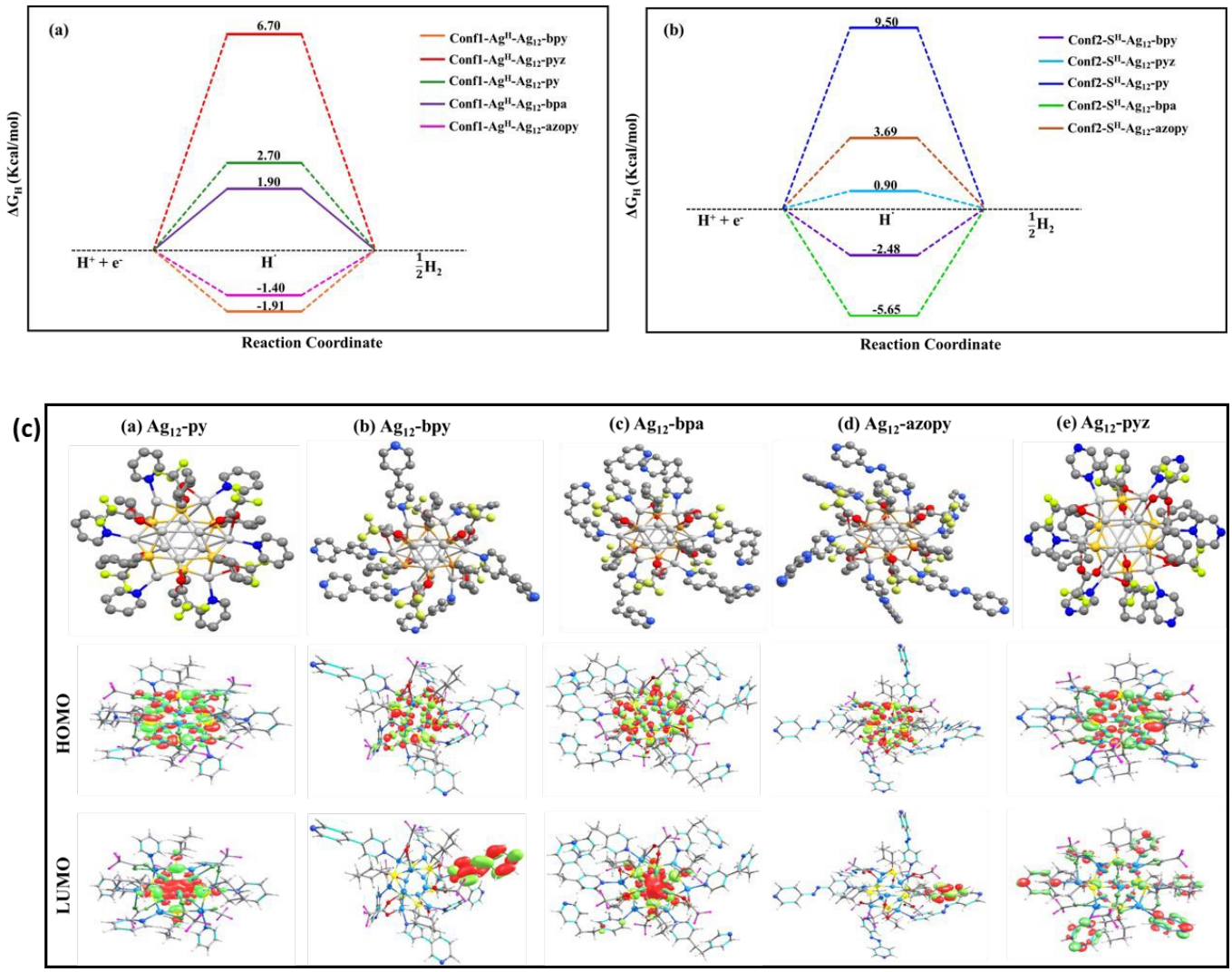

Fig. 4. a) Calculated free energy profile of HER reaction at equilibrium potential (U = U_{RHE}): hydrogen adsorption at the Ag site, (b) hydrogen adsorption at the S site. (c) Optimized structure, occupied and unoccupied molecular orbital, (a) Ag_{12}-py, (b) Ag_{12}-bpy, (c) Ag_{12}-bpa, (d) Ag_{12}-azopy, and (e) Ag_{12}-pyz cluster. color code: Ag, light Grey; S, yellow; O, red; N, blue; C, grey; F, greenish yellow.

Table 1. Calculated ΔG_H values.

ΔG_H (kcal/mol)									
Ag_{12}-pyz		**Ag_{12}-bpy**		**Ag_{12}-bpa**		**Ag_{12}-azopy**		**Ag_{12}-py**	
conf1-Ag^H	conf2-S^H	conf1-Ag^H	conf2-S^H	conf1-Ag^H	conf2-S^H	conf1-Ag^H	conf2-S^H	conf1-Ag^H	conf2-S^H
6.7	0.9	-1.91	-2.48	1.90	-5.65	-1.40	3.69	2.7	9.5

The highest occupied molecular orbitals (HOMO) in these clusters are predominantly localized on the Ag and S atoms, with a minor contribution from the ligand. In contrast, the lowest unoccupied molecular orbitals (LUMO) exhibit a shift from the core of the cluster to the ligand. In Ag_{12}-py and Ag_{12}-bpa, the LUMO is primarily concentrated within the core, while in the Ag_{12}-bpy, Ag_{12}-azopy, and Ag_{12}-pyz clusters, the LUMO is dominated by ligand-centric contributions. This inversion in the distribution of the unoccupied orbital is attributed to the structural variation introduced by the different ligands (Figure 4c). Figure S37 presents the calculated total density of states (TDOS) and partial density of states (PDOS) for these clusters. From the PDOS spectra, it is evident that the valence band in these clusters is primarily occupied by contributions from the core Ag and S atoms, while the conduction band is predominantly influenced by the ligands. As we examine Ag_{12}-bpy, Ag_{12}-bpa, and Ag_{12}-azopy assemblies, the contribution from the ligands in the conduction band increases while the contribution from the Ag-S core decreases. Notably, in the Ag_{12}-pyz, the pyrazine ligand makes a substantial contribution to the conduction band, whereas in the Ag_{12}-py, both the pyridine ligand and the Ag-S core contribute to the conduction band.

Further, observing the theoretical band gap of the assemblies (Table S7), Ag_{12}-pyz manifests a shorter band gap (2.01 eV). This shortest band gap correlates with the favourable experimental conductivity of 4.1×10^{-6} Sm^{-1} (Figure S38). Therefore, it indicates that pyrazine plays a substantial role in the stabilization of the cluster that appears from the lowest LUMOs of the Ag_{12}-pyz CAM. These findings suggest that the electronic structure of the cluster can be effectively manipulated by changing the ligand structure.

From the experimental and theoretical analysis of the cluster structures, we made certain important observations. First, there is a systematic change in the bond distances of Ag-Ag and Ag-S upon variation of the ligand. The experimental crystal structure and theoretical bond length analysis show Ag_{12}-pyz cluster to have a shorter average Ag ... Ag interaction of 2.93 Å (2.89 Å theoretically), compared to others (Table S5 & Figure S35). This might have resulted in a slightly longer Ag—S bond in Ag_{12}-pyz (Table S5). These structural differences corroborate for the observed site preference. The apical S-sites in Ag_{12}-pyz with a higher negative charge, make them more prone to hydrogen compared to others. It is also true that the basicity of the ligands in the series plays an important role in altering the active site based on the electron availability. The higher basicity of py, bpy, bpa, and azopy ligands increases the electron density onto the Ag center, thereby favouring hydrogen adsorption at these sites. However, in the case of pyrazine, the reduced basicity alters the hydrogen adsorption site and maximizes HER activity through the S site. Second, the distribution of canonical orbitals changes, which varies with the ligand, affecting the structure-property relationship. Third, the inter-cluster interactions have a crucial effect on the conductivity of the materials. It has been observed that the material conductivity varies as a function of inter-cluster distance.[53,54] The measured inter-cluster distances are as follows: Ag_{12}-pyz at 7.40 Å, Ag_{12}-bpa at 9.89 Å, Ag_{12}-py at 10.1 Å, Ag_{12}-bpy at 11.38 Å, and Ag_{12}-azopy at 13.36 Å (considering the shortest distance, see figs. S5, S8, S11, S14, S16). The Ag_{12}-pyz with the shortest Ag-Ag inter-cluster distance of 7.4 Å should possess the highest materials conductivity and thereby reflect faster charge transfer kinetics at the electrode-electrolyte interface. Moreover, the isotropic nature (equal in three crystallographic axes) of the Ag-Ag inter-cluster distance in Ag_{12}-pyz, allows the equivalent spatial distribution of the charge transfer process at the interface. In addition, the 3D structure of Ag_{12}-pyz allows effective mass transfer at the interface. However, for the other four sets of cluster assembly, the excessive increase in the Ag-Ag inter-cluster distance (by ~3 Å) (Table S6) does not significantly allow for altered electronic properties (such conductivity) and thereby it can be considered that each Ag-cluster behaves independently. Moreover, the anisotropic behaviour of Ag-Ag inter-cluster distance in different crystallographic directions might act as a barrier for the improved electronic properties. Therefore, it can be said that, for Ag_{12}-pyz the inter-cluster distance and dimensionality have a crucial role over the HER kinetics, while for other clusters the HER kinetics is mainly governed by the H-adsorption energetics. Thus, tuning the ligand can significantly impact the cluster arrangements and the catalytic property. Moreover, we have compared our cluster assemblies with other silver-based NCs catalysts reported in the literature, in terms of the overpotential required for reaching a current density of 10 mA/cm^2 (Table S8). As can be seen, Ag_{12}-pyz displays the best performance among the series.

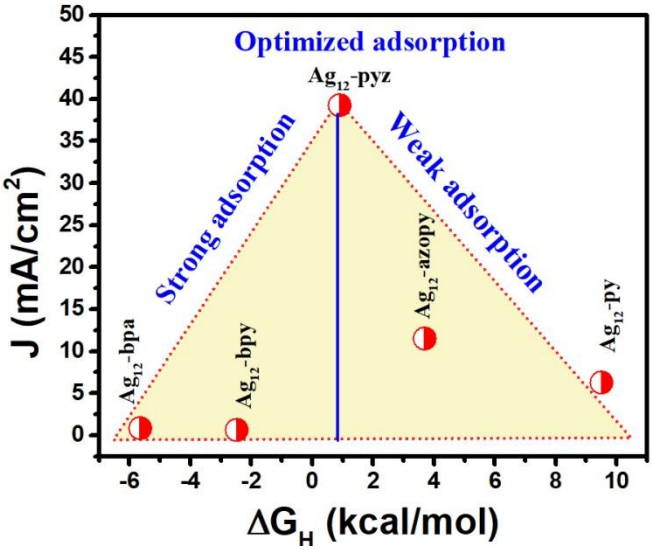

Fig. 5. Volcanic HER activity trend for the five Ag_{12} cluster assemblies.

Experimentally obtained HER activity trend was further rationalized by the current density value at -0.2 V *vs*. RHE against the calculated free energy of H-adsorption (Figure 5). It is well known that for HER, any electrocatalyst with a highly negative ΔG_H value would bind the active H* very strongly and

weakly with a positive ΔG_H value. A very strong and weak H* adsorption would slow down the desorption and adsorption process and thereby reduce the catalytic activity. Hence, H* adsorption with neither too strong nor too weak manner leads to the best catalytic activity according to the 'Sabatier' principle. Here, various nitrogen linkers with their characteristics basicity and electronic structure play a significant role in the H adsorption over S-site and Ag_{12} cluster with pyrazine stabilizer possesses optimum adsorption energy delivering a facile adsorption and desorption process.

Conclusions

In this study, five assemblies were studied: Ag_{12}-py, Ag_{12}-pyz, Ag_{12}-bpy, Ag_{12}-bpa, Ag_{12}-azopy. The Ag_{12}-pyz showed superior catalytic activity for HER compared to others in the series. Theoretical analysis on hydrogen adsorption free energy showed more favourable hydrogen adsorption for the Ag_{12}-pyz case, enhancing HER performance compared to others. Further, the active center for catalytic hydrogen adsorption in Ag_{12}-pyz was observed to be at the apical S site, while it is at the Ag—Ag site for the other 4 assemblies. This alteration of the active site is attributed to intercluster assembly and the basicity of the linker. The isotropic nature of the Ag-Ag inter-cluster distance in Ag_{12}-pyz, allows the equivalent spatial distribution of the charge transfer process. The relatively less basic pyrazine linker renders the silver more electropositive, and a conclusion also supported by structural analysis, which showed the shortest Ag— Ag interactions in the Ag_{12}-pyz, thus favoring its positioning at the apical S site. The variations in catalytic activity and active site preference among these assemblies were achieved by systematically altering the ligands from pyridine to azopyridine. This work, offering a molecular-level correlation of linker-induced assembly, the activity and active site switching in cluster assemblies, highlights a significant toolkit for selectively designing cluster assemblies as catalysts that hold broad implications for tailored catalytic activity in various applications.

Author contributions

The manuscript was written through the contributions of all authors. All authors have given approval to the final version of the manuscript.

Data availability

Supporting Information contains details on synthesis, crystallographic information, optical images, crystal structure details, PXRD, SEM, XPS, TGA, post-catalytic analysis, DFT results, I-V characteristics, comparison table, references and optimized coordinates.

Conflicts of interest

The authors declare no competing financial interest.

Acknowledgements

C.P Acknowledge the Council of Scientific & Industrial Research India for fellowship. We acknowledge the fund by a grant from the Italian Ministry of Foreign Affairs and International Cooperation and the Indian Department of Science & Technology. K. B. acknowledges the IITG start-up grant and PARAM KAMRUPA for computational facilities. The authors acknowledge Dr. A. Mukherjee and S. K. Singh for their assistance during I-V measurements. CSIR-CECRI MS reference number # CECRI/PESVC/Pubs/2024-045. We acknowledge the Science Engineering and Research Board through the grants CRG/2022/ 000984. Authors acknowledge V. Nandana and M. Rahul for their help during synthesis.

References

1 I. Chakraborty and T. Pradeep, *Chem. Rev.*, 2017, **117**, 8208–8271.
2 R. Jin and T. Higaki, *Commun. Chem.*, 2021, **4**, 6–9.
3 Y. Lu and W. Chen, *Chem. Soc. Rev.*, 2012, **41**, 3594–3623.
4 X. Kang and M. Zhu, *Chem. Soc. Rev.*, 2019, **48**, 2422–2457.
5 O. J. H. Chai, Z. Liu, T. Chen and J. Xie, *Nanoscale*, 2019, **11**, 20437–20448.
6 K. Kwak and D. Lee, *Acc. Chem. Res.*, 2019, **52**, 12–22.
7 H. Yan, H. Xiang, J. Liu, R. Cheng, Y. Ye, Y. Han and C. Yao, *Small*, 2022, **18**, 1–21.
8 Y. Du, H. Sheng, D. Astruc and M. Zhu, *Chem. Rev.*, 2020, **120**, 526–622.
9 K. Kwak, W. Choi, Q. Tang, M. Kim, Y. Lee, D. Jiang and D. Lee, *Nat. Commun.*, 2017, **8**, 14723.
10 Z. Liu, H. Tan, B. Li, Z. Hu, D. Jiang, Q. Yao, L. Wang and J. Xie, *Nat. Commun.*, 2023, **14**, 3374.
11 T. Kawawaki, A. Ebina, Y. Hosokawa, S. Ozaki, D. Suzuki, S. Hossain and Y. Negishi, *Small*, 2021, **17**, 2005328.
12 R. Jin, G. Li, S. Sharma, Y. Li and X. Du, *Chem. Rev.*, 2021, **121**, 567–648.
13 J. Ding, H. Yang, S. Zhang, Q. Liu, H. Cao, J. Luo and X. Liu, *Small*, 2022, **18**, 2204524.
14 D. K. Jangid, S. G. Dastider, R. Biswas, S. Khirid, S. Meena, P. Kumar, S. C. Sahoo, V. P. Verma, R. D. Makde, A. Kumar, R. Jangir, K. Mondal, K. K. Haldar and R. S. Dhayal, *Inorg. Chem.*, 2022, **61**, 13342–13354.
15 S. Dai, T. Kajiwara, M. Ikeda, I. Romero-Muñiz, G. Patriarche, A. E. Platero-Prats, A. Vimont, M. Daturi, A. Tissot, Q. Xu and C. Serre, *Angew. Chemie. Int. Ed.*, 2022, **61**, e202211848.
16 H. Wang, X. Zhang, W. Zhang, M. Zhou and H.-L. Jiang, *Angew. Chemie Int. Ed.*, 2024, **63**, e202401443.
17 J. V. Rival, P. Mymoona, K. M. Lakshmi, Nonappa, T. Pradeep and E. S. Shibu, *Small*, 2021, **17**, 1–33.
18 Z. Wang, X.-Y. Li, L.-W. Liu, S.-Q. Yu, Z.-Y. Feng, C.-H. Tung and D. Sun, *Chem. – A Eur. J.*, 2016, **22**, 6830–6836.
19 S.-S. Zhang, X. Wang, H.-F. Su, L. Feng, Z. Wang, W.-Q. Ding, V. A. Blatov, M. Kurmoo, C.-H. Tung, D. Sun and L.-S. Zheng, *Inorg. Chem.*, 2017, **56**, 11891–11899.
20 Y. Jin, C. Zhang, X. Y. Dong, S. Q. Zang and T. C. W. Mak,

Chem. Soc. Rev., 2021, **50**, 2297–2319.

21 A. Ebina, S. Hossain, H. Horihata, S. Ozaki, S. Kato, T. Kawawaki and Y. Negishi, *Nanomaterials*, 2020, **10**, 1105.

22 X. Kang and M. Zhu, *Coord. Chem. Rev.*, 2019, **394**, 1–38.

23 S. A. Claridge, A. W. Castleman, S. N. Khanna, C. B. Murray, A. Sen and P. S. Weiss, *ACS Nano*, 2009, **3**, 244–255.

24 S. Bonacchi, S. Antonello, T. Dainese and F. Maran, *Chem. – A Eur. J.*, 2021, **27**, 30–38.

25 P. Chandrashekar, G. Sardar, T. Sengupta, A. C. Reber, P. K. Mondal, D. Kabra, S. N. Khanna, P. Deria and S. Mandal, *Angew. Chemie Int. Ed.*, 2023, **63**, e202317345.

26 R. W. Huang, Y. S. Wei, X. Y. Dong, X. H. Wu, C. X. Du, S. Q. Zang and T. C. W. Mak, *Nat. Chem.*, 2017, **9**, 689–697.

27 S. Wang, A. Lu and C.-J. Zhong, *Nano Converg.*, 2021, **8**, 4.

28 T. B. Ferriday, P. H. Middleton and M. L. Kolhe, *Energies*, 2021, **14**, 8535.

29 Y. Zheng, Y. Jiao, M. Jaroniec and S. Z. Qiao, *Angew. Chemie Int. Ed.*, 2015, **54**, 52–65.

30 Y. Li, S. Li, A. V. Nagarajan, Z. Liu, S. Nevins, Y. Song, G. Mpourmpakis and R. Jin, *J. Am. Chem. Soc.*, 2021, **143**, 11102–11108.

31 J. Cai, R. Javed, D. Ye, H. Zhao and J. Zhang, *J. Mater. Chem. A*, 2020, **8**, 22467–22487.

32 L. Chang, D. Cheng, L. Sementa and A. Fortunelli, *Nanoscale*, 2018, **10**, 17730–17737.

33 X. Yuan and M. Zhu, *Inorg. Chem. Front.*, 2023, **10**, 3995–4007.

34 R. P. Brocha Silalahi, Y. Jo, J. Liao, T. Chiu, E. Park, W. Choi, H. Liang, S. Kahlal, J. Saillard, D. Lee and C. W. Liu, *Angew. Chemie Int. Ed.*, 2023, **62**, e202301272.

35 T. Imaoka, H. Kitazawa, W.-J. Chun, S. Omura, K. Albrecht and K. Yamamoto, *J. Am. Chem. Soc.*, 2013, **135**, 13089–13095.

36 X. Wang, L. Zhao, X. Li, Y. Liu, Y. Wang, Q. Yao, J. Xie, Q. Xue, Z. Yan, X. Yuan and W. Xing, *Nat. Commun.*, 2022, **13**, 1596.

37 Y. Tang, F. Sun, X. Ma, L. Qin, G. Ma, Q. Tang and Z. Tang, *Dalt. Trans.*, 2022, **51**, 7845–7850.

38 G. Ma, Y. Tang, L. Chen, L. Qin, Q. Shen, L. Wang and Z. Tang, *Eur. J. Inorg. Chem.*, 2022, **21**, e202200176.

39 W. Choi, G. Hu, K. Kwak, M. Kim, D. Jiang, J.-P. Choi and D. Lee, *ACS Appl. Mater. Interfaces*, 2018, **10**, 44645–44653.

40 H. Shen, Q. Zhu, J. Xu, K. Ni, X. Wei, Y. Du, S. Gao, X. Kang and M. Zhu, *Nanoscale*, 2023, **15**, 14941–14948.

41 M. Ghosal Chowdhury, L. Sahoo, S. Maity, D. Bain, U. K. Gautam and A. Patra, *ACS Appl. Nano Mater.*, 2022, **5**, 7132–7141.

42 M. A. Abbood, R. H. Althomali, F. Al-dolaimy, R. M. Portilla, S. S. Abdullaev, M. Del Carmen Delgado Laime, Z. F. Hassan, A. hussien R. Abbas and A. H. Alsaalamy, *Ionics (Kiel).*, 2024, **30**, 433–444.

43 Z. Wang, R. K. Gupta, F. Alkan, B.-L. Han, L. Feng, X.-Q. Huang, Z.-Y. Gao, C.-H. Tung and D. Sun, *J. Am. Chem. Soc.*, 2023, **145**, 19523–19532.

44 Y. Wang, X.-K. Wan, L. Ren, H. Su, G. Li, S. Malola, S. Lin, Z. Tang, H. Häkkinen, B. K. Teo, Q.-M. Wang and N. Zheng, *J. Am. Chem. Soc.*, 2016, **138**, 3278–3281.

45 G. Hu, Q. Tang, D. Lee, Z. Wu and D. Jiang, *Chem. Mater.*, 2017, **29**, 4840–4847.

46 X. Cai, Y. Sun, J. Xu and Y. Zhu, *Chem. – A Eur. J.*, 2021, **27**, 11539–11547.

47 B. Kumar, T. Kawawaki, N. Shimizu, Y. Imai, D. Suzuki, S. Hossain, L. V. Nair and Y. Negishi, *Nanoscale*, 2020, **12**, 9969–9979.

48 M. H. Naveen, R. Khan and J. H. Bang, *Chem. Mater.*, 2021, **33**, 7595–7612.

49 O. López-Estrada, N. Mammen, L. Laverdure, M. M. Melander, H. Häkkinen and K. Honkala, *ACS Catal.*, 2023, **13**, 8997–9006.

50 F. Sun, Q. Tang and D. Jiang, *ACS Catal.*, 2022, **12**, 8404–8433.

51 A. Karmakar, M. Durairaj, R. Madhu, A. De, H. N. Dhandapani, M. J. S. Spencer and S. Kundu, *ACS Mater. Lett.*, 2024, **6**, 3050–3062.

52 E. Skúlason, G. S. Karlberg, J. Rossmeisl, T. Bligaard, J. Greeley, H. Jónsson and J. K. Nørskov, *Phys. Chem. Chem. Phys.*, 2007, **9**, 3241–3250.

53 R. Tsunashima, I. Nakamura, R. Oue, S. Koga, H. Oki, S. Noro, T. Nakamura and T. Akutagawa, *Dalt. Trans.*, 2017, **46**, 12619–12624.

54 C. Bansal, S. G. Praveen, J. T. T. Kumaran and A. Chatterjee, *Sci. Rep.*, 2015, **5**, 7685.

View Article Online
DOI: 10.1039/D4SC08408J

Data availability statement

The data will be available from the authors on request for academic purpose.